The Canadian Mineralogist
Vol. 38, pp. 101-117 (2000)

As-BEARING FLUORAPATITE IN MANGANIFEROUS DEPOSITS FROM ST. MARCEL – PRABORNA, VAL D'AOSTA, ITALY

ELENA-ADRIANA PERSEIL

Laboratoire de Minéralogie, Muséum National d'Histoire Naturelle, ESA–CNRS 7058, 61, rue Buffon, F-75005 Paris, Cedex 05, France

PHILIPPE BLANC[§]

Service Commun de Microscopie Electronique, ESA–CNRS 7073, Boîte 104, Université Pierre et Marie Curie, 4, place Jussieu, F-75252 Paris Cedex 05, France

DANIEL OHNENSTETTER

Centre National de Recherches Scientifiques, Centre de Recherches Pétrographiques et Géochimiques, 15, rue Notre-Dame-des-Pauvres, BP 20, F-54501 Vandoeuvre-lès-Nancy Cedex, France

Abstract

We describe important variations in the crystal chemistry of fluorapatite from the manganiferous deposit at the St. Marcel – Praborna mine in the Val d'Aosta, Italy. Three types of fluorapatite were observed. Their cathodoluminescence, coupled with *in situ* electron-microprobe analyses, reveal a direct relationship between the intensity of cathodoluminescence and the concentration of Mn^{2+} and As^{5+}. The progressive replacement of P by As and of Ca by Sr, linked to the fracturing of the minerals and circulation of fluid, has been observed in the latest-stage apatite. Arsenic efficiently quenches the luminescence due to the incorporation of trace amounts of the rare-earth elements, and only partially quenches emission due to high concentrations of Mn^{2+}. A drastic increase in As, up to 10 wt% As_2O_5, quenches all luminescence.

Keywords: fluorapatite, cathodoluminescence, rare-earth elements, electron-microprobe analysis, arsenic, quencher, St. Marcel – Praborna, Italy.

Sommaire

Nous décrivons d'importantes variations dans la cristallochimie de la fluorapatite des concentrations manganésifères de la mine de St. Marcel – Praborna dans le Val d'Aoste, Italie. Trois types de fluorapatite ont pu être distingués. L'observation de leur propriétés de luminescence couplée à la microanalyse *in situ* par sonde électronique permet de mettre en évidence une relation directe entre l'intensité de cathodoluminescence et la concentration en Mn^{2+} et As^{5+}. Un remplacement progressif du P par l'As et du Ca par le Sr, associés à une forte fracturation des minéraux et à la circulation de fluides, a été observé dans l'apatite la plus tardive. L'effet inhibiteur de l'arsenic est total vis-à-vis des émissions de luminescence dues à l'incorporation des terres rares à l'état de traces, alors qu'il n'est que partiel pour l'émission due à la présence de fortes concentrations en Mn^{2+}. Par contre, l'augmentation drastique des teneurs en As, pouvant atteindre jusqu'à 10% As_2O_5 poids, fait disparaître toute luminescence.

Mots-clés: fluorapatite, cathodoluminescence, terres rares, microanalyse par sonde électronique, arsenic, effet d'inhibition de la luminescence, St. Marcel – Praborna, Italie.

Introduction

Arsenic-bearing apatite has been found in metamorphosed manganiferous ores in the western Italian Alps at St. Marcel – Praborna (Perseil & Smith 1996), and in the Eastern Swiss Alps at Val Ferrera (Brugger & Gieré 1999). Pentavalent As is known to partly replace P^{5+} in the tetrahedral site in fermorite (Hughes & Drexler 1991) or to totally replace it in johnbaumite, the arsenate analogue of hydroxylapatite, and in svabite, the fluorarsenate analogue of fluorapatite (Dunn *et al.* 1980). The main substitutions in apatite are the replace-

§ To whom correspondence should be addressed. *E-mail address*: blancmeb@ccr.jussieu.fr

ment of Ca^{2+} by Mn^{2+}, Sr^{2+} and the rare-earth elements (*REE*). Strontium enters only the Ca(2) site, whereas Mn^{2+} enters both Ca sites, but preferentially the larger [*i.e.*, Ca(1)] site (Hughes *et al.* 1991a); the *REE* show a marked preference for the low-symmetry Ca(2) site (Morozov *et al.* 1970, Tarashchan 1978, Hughes *et al.* 1991b, Fleet & Pan 1995). Eu^{3+}, where present, occurs in the high-symmetry Ca(1) site (Gaft *et al.* 1997). The incorporation of the rare-earth elements (*REE*) in apatite requires charge compensation, either by O^{2-} replacing F (Morozov *et al.* 1970), or by coupled substitution of REE^{3+} + Na^{+} replacing 2 Ca^{2+} (Efimov *et al.* 1962, Roeder *et al.* 1987, Rønsbo 1989) or REE^{3+} + Si^{4+} replacing Ca^{2+} + P^{5+} (Rønsbo 1989) or by 2 REE^{3+} + □ replacing 3 Ca^{2+} (Fleet & Pan 1995). Our aim in this paper is to elucidate the As-bearing fluorapatite from St. Marcel – Praborna, Italy, and its geological environment, and to correlate crystal chemistry and cathodoluminescence (CL) emission spectroscopy.

Geological Setting and Previous Findings

The St. Marcel – Praborna mine is located in the Val d'Aosta, in the western Italian Alps, and belongs to the lower part of the Piedmont Jurassic ophiolitic nappe, of oceanic origin (Martin-Vernizzi 1982). The manganiferous deposits are enclosed in chert, transformed to quartzite in the basal part of the post-ophiolitic sedimentary cover (Debenedetti 1965, Dal Piaz *et al.* 1979). The ophiolites and their sedimentary cover were metamorphosed to the eclogitic facies (Martin-Vernizzi 1982, Mottana 1986, Martin & Kienast 1987). The manganiferous cherts have been transformed to banded quartzites and pyroxenites. Lenses of massive Mn ores composed of braunite and accessory hausmannite are included in the pyroxenites as fine-grained braunite–quartz rocks. Braunite is the predominant oxide in this deposit; it is commonly associated with a member of the cryptomelane–hollandite series.

The complex metamorphic evolution and the specific mineral assemblage were described in detail by Perseil (1988, 1991) and Perseil & Smith (1995). The pressure–temperature (P–T) path of metamorphism is subdivided into four main stages (Martin-Vernizzi 1982). The first stage ("A") is a relict pre-eclogitic blueschist containing lawsonite and Na–Ca amphiboles included in late eclogitic garnet, comparable to the parageneses described by Brown *et al.* (1979), who estimated a pressure of 8 kbar and a temperature of 350 ± 50°C. The second stage ("B") is a prograde eclogite-facies metamorphism reaching a temperature between 450 and 480°C according to the clinopyroxene–garnet geothermometer (Ellis & Green 1979) and a pressure of 8.5–10 kbar estimated from the activity of the jadeite component in the clinopyroxene (Holland 1980). The third stage ("C") is a post-eclogitic blueschist paragenesis, with development of Na-amphiboles instead of omphacite. The temperature is estimated to have been 400°C using the albite–microcline geothermometer (Whitney & Stormer 1977), and the pressure is estimated using the phengitic substitution in the trioctahedral micas (Velde 1967) at 7 kbar. The same P and T were estimated for the Breuil – St. Jacques area nearby (Ernst & Dal Piaz 1978). The last metamorphic event ("D") led to the development of a greenschist-facies overprint in shear zones during the last stage of deformation. The P and T of this event are estimated using the Mn-in-carbonate geothermobarometer (Peters *et al.* 1978) at 450°C and <6 kbar. The presence of apatite was mentioned in previous studies (Burckhardt & Falini 1956, Brown *et al.* 1979, Martin-Vernizzi 1982); however, no study was undertaken of the crystal chemistry of this mineral or of its habit and its petrographic occurrences.

Petrography and Mineralogy of the Fluorapatite-Bearing Rocks

In the quartzites, two different horizons were observed; the first is emerald-green, whereas the second is grey to pink. Late veinlets cross-cutting the manganiferous ores are faulted. It is in these veinlets that the As-bearing fluorapatite occurs. The emerald-green quartzitic horizon is a feldspathic quartzite composed of large crystals of albite, green chromian aegirine–augite (Morimoto 1989), titanite, calcite, green tremolite (Leake *et al.* 1997), green chlorite, Cr-bearing magnetite and fluorapatite. The grey to pink quartzite is composed of braunite, spessartine, piemontite and quartz. In the greenschist episode, the garnet – braunite – quartz association is stable only above 600°C (Huebner 1977), higher than the eclogitic isotherm, estimated between 400 and 500°C (Martin-Vernizzi 1982). Close to the late albite and calcite veinlets, As-bearing fluorapatite is euhedral or anhedral and contains numerous cracks (Fig. 1f). As- and Sb-bearing titanite (Perseil & Smith 1995), Sb-rich rutile (Perseil 1991), and piemontite are associated with the fluorapatite. Optical and CL microscopy (see appendix for analytical methods) reveal three types of apatite within these rocks.

Characterization of the Three Types of As-Bearing Fluorapatite

Fluorapatite of type I, with a bright CL emission

Such fluorapatite is euhedral to subhedral, from 50 to 600 μm in size. It is slightly rounded and contains cracks, which may locally be abundant. This type of fluorapatite occurs in thin bands that are located near late albite and carbonate veinlets in both emerald-green and grey to pink quartzites. The fluorapatite of type I contains numerous inclusions of quartz, rutile, titanite, and piemontite. In the grey to pink horizon, the fluorapatite is <100 μm in size, has a bright yellow luminescence (Fig. 1e) and encloses zircon. Luminescence is very characteristic of the first type of fluorapatite. Its

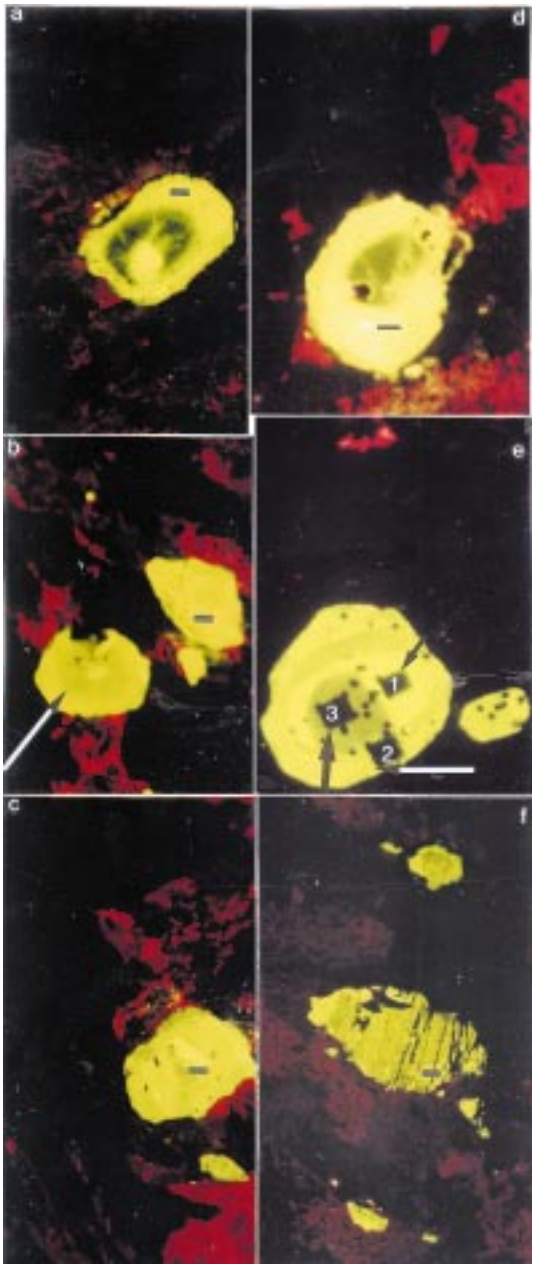

FIG. 1. Cathodoluminescence images of fluorapatite of type I. a–d. Fluorapatite from the emerald- green quartzite horizon (sample S.M. 23–1) showing complex zoning, indicated by the change in color from bright yellow to green-yellow and, in some cases, nonluminescent zones (a). The crystal in the center of the photograph in b (arrow) was also analyzed with SEM–CL imagery (Fig. 2) and CL spectrometry (Fig. 4). In a, b, and c, the scale bar (on the apatite grain) is 50 μm. Note that the red CL patches in Figure 1 are due to the luminescence of calcite and albite. d. Oscillatory growth-induced zoning in fluorapatite of type I (sample S.M. 23–1) showing a nonluminescent core. The scale bar is 100 μm. e. Fluorapatite of type I in the grey to pink quartzite horizon (sample S.M. 98–2) with very bright yellow CL. The same grain under the SEM and its BSE and CL images are given in Figure 3. Each rectangle is 40 μm wide and corresponds to the CL spectrum recorded on SEM and each spot to the EPMA analysis. Scale bar: 100 μm. f. Fluorapatite of type I with microcracks (sample S.M. 96–7), associated with sodic pyroxene close to the late veins and showing a bright yellow emission. The CL variations are linked to the microcracks. The scale bar is 100 μm. The same grain is shown in SEM BSE and X-ray images (Fig. 6), and the CL spectrum is given in Figure 7.

intensity is highest, and oscillatory growth-induced zoning is clearly developed, with a succession of brighter and darker zones. In general, the bright zones occur in the center of the mineral, overgrown by a succession of dark zones (Figs. 1a, b, e, 2). The various zones show a bright yellow color that grades to yellow-green (Figs. 1a, b, c). In some cases, the dark zone is located in the center of the crystal (Fig. 1d). The oscillatory growth-zones vary from 10 nm to 10 μm across. In the emerald-green (Figs. 1a, b, d) or in the grey to pink quartzite horizon (Fig. 1e), the subhedral fluorapatite shows obvious growth zoning. Close to the albite and calcite veinlets, the anhedral fluorapatite contains numerous cracks; a variation in CL intensity is noted along the cracks and fissures. The less intensely luminescent areas are close to the cracks (Fig. 1f), and may be related to late circulation of fluid.

The oscillatory growth-zoning is also revealed on back-scattered electron (BSE) images and X-ray maps (Figs. 2, 3). BSE images (Fig. 2a) confirm the oscillatory zoning observed on CL images (Fig. 2b). In the emerald-green quartzite, the bright zones on the BSE image, which correspond to the higher mean atomic number (Z), are also less luminescent (Fig. 2). In the analyzed crystals of fluorapatite (see appendix for details of the analytical methods), the increase in Z is due to the presence of As. In the grey to pink quartzite horizon, the zoning in the fluorapatite is more marked, and the high-Z zones on the BSE images are brighter than in the emerald-green quartzite horizon (Fig. 3a). These crystals of fluorapatite may contain very strongly luminescent grains of zircon (Fig. 3b). The bright center on the BSE image (Fig. 3a), which corresponds to the less luminescent area in the CL image (Fig. 3b), is linked to the substitution of P by As, as confirmed by X-ray mapping (Fig. 3c).

The CL spectra (see appendix for details of the analytical methods) of the bright zones from fluorapatite from the emerald-green quartzite horizon show a large band centered between 560 and 580 nm (Fig. 4) due to the Mn^{2+} activator (Portnov & Gorobets 1969, Mariano & Ring 1975, Roeder *et al.* 1987, Blanc *et al.* 1995,

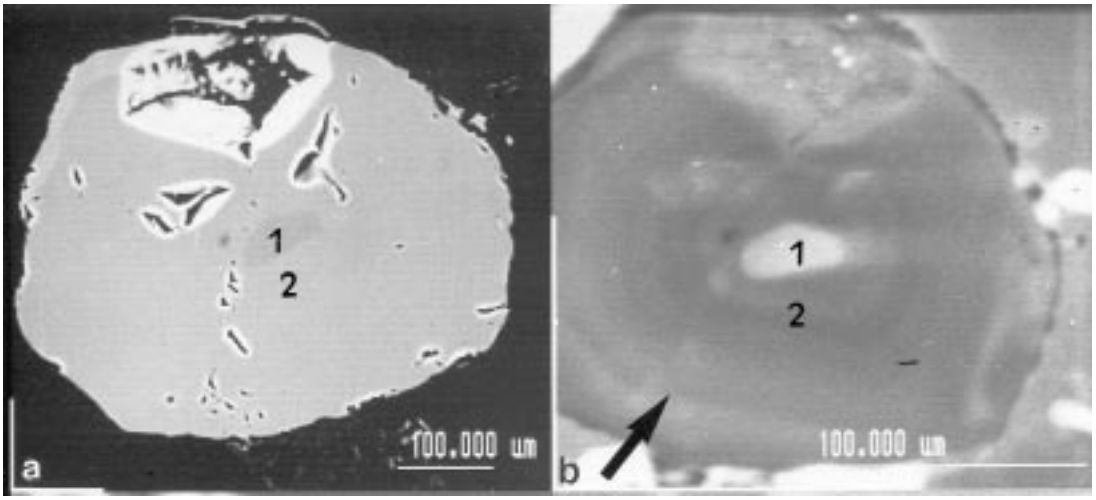

FIG. 2. Fluorapatite of type I. a. BSE image of fluorapatite of type I from the emerald-green quartzite horizon corresponding to the yellow CL fluorapatite in b. Note the weak contrast between the core and the rim. On the contrary, in the CL image of the same grain (b), the core is well defined, as are the different oscillatory growth-zones (arrow). Areas 1 and 2 indicate where the CL spectra (Fig. 4) were recorded.

Mitchell *et al.* 1997), and correspond to the d–d $^4T_{1g} \rightarrow {}^6A_{1g}$ electronic transition (Tarashchan 1978, Marfunin 1979). In the fluorapatite from the emerald-green quartzite horizon, the high concentration of Mn^{2+} is accompanied by a high content of the rare-earth elements (*REE*). Such high *REE* concentrations induce CL emission of sharp lines that overlap the large Mn^{2+} band centered at 576 nm (Blanc *et al.* 1995, Mitchell *et al.* 1997). They correspond to *f*–*f* electronic transitions (Tarashchan 1978, Marfunin 1979). In the As-bearing zones within this apatite, the CL emission lines of the *REE* do not appear, and emission by the *REE* are quenched by the presence of As in the structure.

In the fluorapatite from the grey to pink quartzite horizon, the extent of substitution of P by As is shown by an X-ray map (Fig. 3c). On CL spectra recorded under the same experimental conditions, the Mn peak decreases with the increase of the As-for-P substitution (Fig. 5). Thus it seems that As is a CL quencher in fluorapatite. The same phenomenon is observed in the anhedral grains of fluorapatite close to the veinlets, the patchy zoning being due to fluid circulation along cracks (Fig. 6a). The high As (Fig. 6b) and low P (Fig. 6c) contents are located in the high-Z areas on the BSE images (Fig. 6a), and the As distribution is linked to late circulation of fluid. The CL spectrum of this type of fluorapatite (Fig. 7) is similar to that in the emerald-green quartzitic horizon (Fig. 4).

The more strongly luminescent fluorapatite from the emerald-green quartzite horizon contains traces of Mn and Sr, whereas As is very low to absent (Table 1). In the grey to pink quartzite horizon, the compositional variation in the fluorapatite is greater (Table 2). The

TABLE 1. COMPOSITION* OF TYPE-I FLUORAPATITE FROM THE EMERALD-GREEN QUARTZITE HORIZON OF THE ST. MARCEL – PRABORNA DEPOSIT

Sample number	S.M. 23–1 1	2	3	4	5	6
P_2O_5 wt%	43.10	41.97	42.06	41.19	41.36	41.88
As_2O_5	0.00	0.17	0.39	0.57	1.16	1.30
V_2O_5	0.00	0.00	0.00	0.15	0.00	0.00
SiO_2	0.03	0.00	0.00	0.00	0.00	0.06
TiO_2	0.10	0.00	0.00	0.08	0.05	0.00
Al_2O_3	0.04	0.00	0.00	0.00	0.00	0.00
FeO	0.00	0.00	0.00	0.00	0.09	0.01
MnO	0.03	0.00	0.00	0.05	0.17	0.19
CaO	55.75	56.38	55.16	56.00	56.03	55.50
SrO	0.03	0.01	0.00	0.17	0.16	0.17
F	2.90	2.90	2.46	2.68	2.83	2.83
Cl	0.00	0.00	0.00	0.00	0.00	0.00
H_2O calculated	0.44	0.42	0.62	0.51	0.45	0.46
–O=F	1.22	1.22	1.04	1.13	1.19	1.19
–O=Cl	0.00	0.00	0.00	0.00	0.00	0.00
Total	101.20	100.63	99.65	100.27	101.11	101.21
Structural formulae based on (P + As + V + Si + Ti + Al) = 6 atoms, (Fe + Mn + Ca + Sr) = 10 atoms and (F + Cl + OH) = 2 atoms						
P *apfu*	5.982	5.985	5.966	5.922	5.892	5.877
As	0.000	0.015	0.034	0.051	0.102	0.113
V	0.000	0.000	0.000	0.017	0.000	0.000
Si	0.005	0.000	0.000	0.000	0.000	0.010
Ti	0.012	0.000	0.000	0.010	0.006	0.000
Al	0.001	0.000	0.000	0.000	0.000	0.000
Fe	0.000	0.000	0.000	0.000	0.012	0.001
Mn	0.004	0.000	0.000	0.007	0.024	0.027
Ca	9.993	9.999	10.000	9.977	9.948	9.955
Sr	0.003	0.001	0.000	0.016	0.015	0.017
F	1.516	1.534	1.309	1.428	1.497	1.490
Cl	0.000	0.000	0.000	0.000	0.000	0.000
OH	0.484	0.466	0.691	0.572	0.503	0.510

1: bright yellow CL hue; 2–6: yellow CL hue. * Electron-microprobe data. *apfu*: atoms per formula unit.

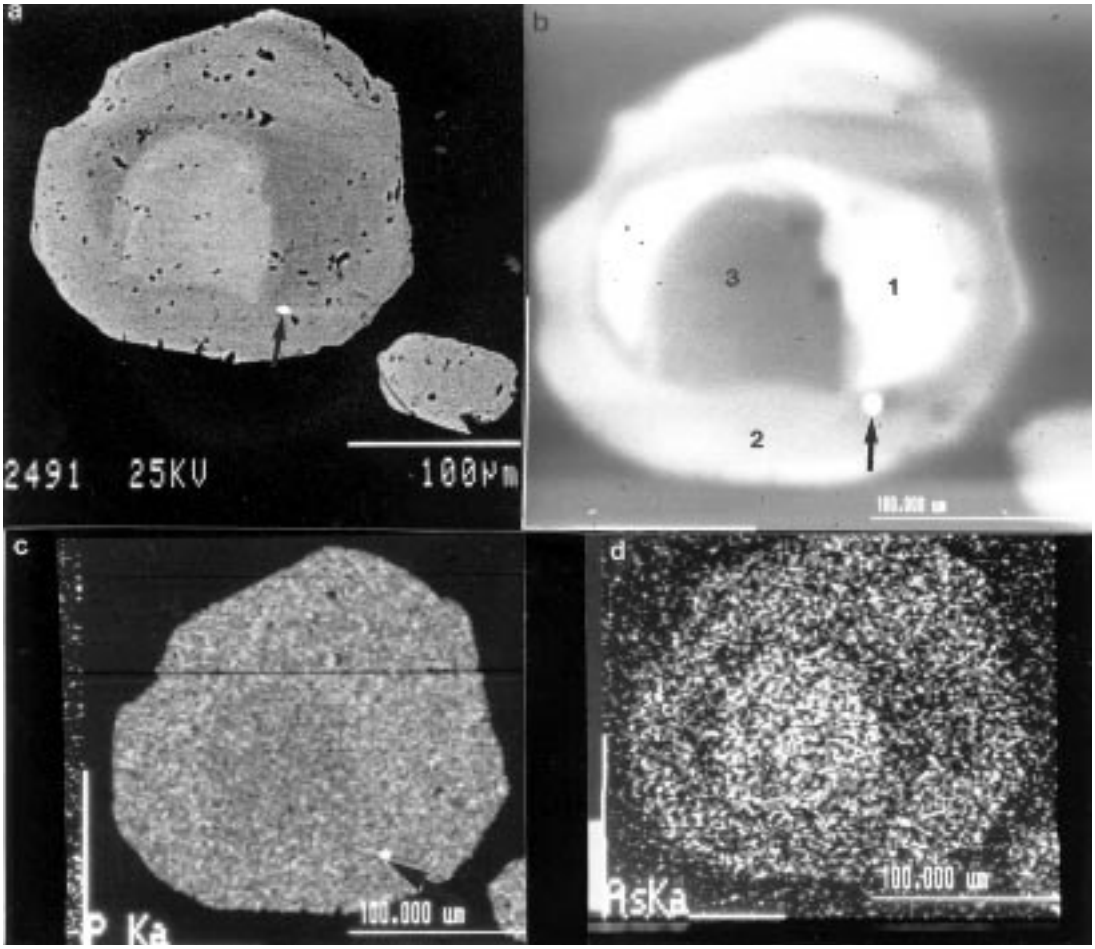

FIG. 3. Fluorapatite of type I. a. BSE image of fluorapatite of type I from the grey to pink quartzite horizon corresponding to the bright yellow CL fluorapatite on Figure 1e. Note the contrast between the core and the various oscillatory growth-zones on both BSE (a) and CL (b) images. The dark CL core is due mainly to the replacement of P (c) by As (d), as shown by the X-ray maps. Areas 1 to 3 indicate where the CL spectra (Fig. 5) were recorded. Note that the fluorapatite grain contains a brightly luminescent grain of zircon (arrow) visible on BSE (a), CL (b) and P (+ Zr) X-ray map (c).

luminescent zones show a high concentration of Sr (Table 2, anal. 1), whereas in the dark CL center (Fig. 3b), the Sr content decreases and As_2O_5 reaches 9.55 wt%. In the fluorapatite close to the veinlets, a slight increase in Sr coupled with a strong increase in As (Table 3) is observed. The substitution of P by As is limited in the fluorapatite of type I from this emerald-green horizon. The chemical variation in the type-I fluorapatite from the grey to pink quartzitic layers is more marked, as revealed in their BSE images. The most luminescent areas show the highest Sr content (Table 2, anal. 1), whereas the Mn content is below the detection limit (<10 ppm) of the electron microprobe in the core, which appears dull under CL (Fig. 3b). A strong increase in As content is coupled with a decrease in Sr content. On the contrary, the composition of the fluorapatite close to the veinlets (Table 3) exhibits an increase in both As and Sr contents. The highest values of both elements are restricted to areas close to the fractures, indicating that their enrichment is probably due to late circulation of fluid. The highest As values are correlated with a decrease of Mn and an increase of Sr and Si. In the first type of fluorapatite from St. Marcel – Praborna, there is a direct link between the extent of substitution of P by As and the decrease in intensity of the luminescence, but the crystals are never completely dull.

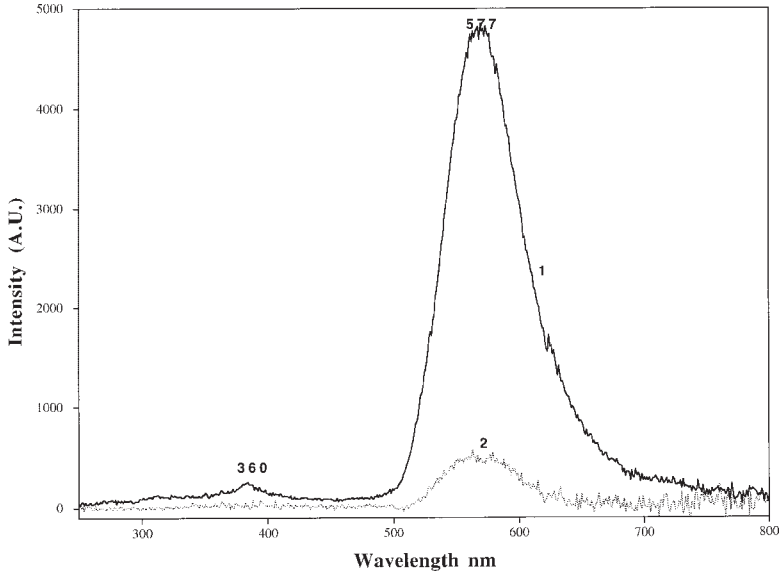

FIG. 4. CL spectra of the fluorapatite crystal shown in Figures 1b and 2, and determined on the most luminescent zone (spectrum 1), and on the least luminescent zone (spectrum 2). The operating conditions were: voltage: 25 kV, beam intensity: 1×10^{-7} A, spectrometer slits: 1 mm, range of wavelength: 200 to 900 nm (see Appendix for more details). Intensity in arbitrary units (A.U.).

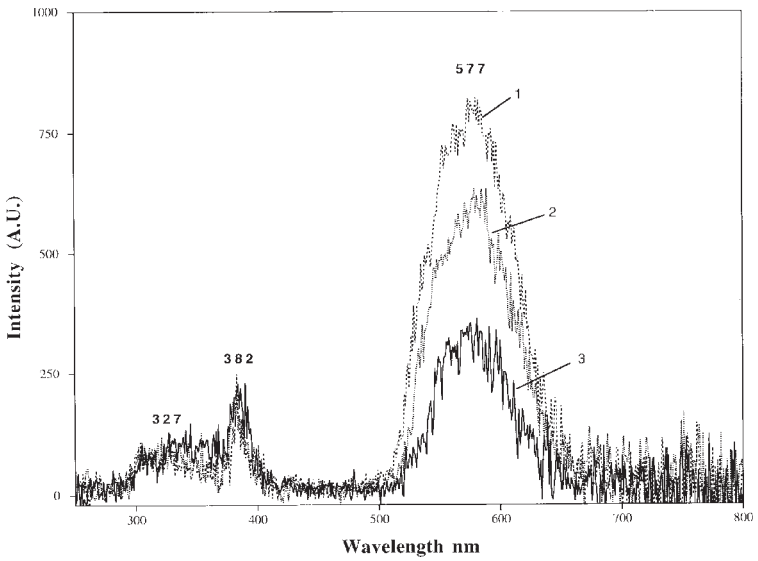

FIG. 5. CL spectra of the fluorapatite crystal shown in Figures 1e and 3b. Same operating conditions as in Figure 4. The most intense spectrum (1) corresponds to the rim (Fig. 3b), and the least luminescent spectrum (3), to the core of the crystal (Figs. 3b, c). The intensity of the Mn^{2+} peak at 577 nm decreases drastically from core to rim; the emissions in the UV domain are nearly constant.

TABLE 2. COMPOSITION* OF TYPE-I FLUORAPATITE FROM THE BASAL GREY TO PINKISH QUARTZITE UNIT OF THE ST. MARCEL – PRABORNA DEPOSIT

Sample number	S.M. 98–2 1	2	3	4	5	6
P_2O_5 wt%	41.70	38.44	36.25	36.05	34.55	34.22
As_2O_5	0.91	4.26	6.32	7.51	8.63	9.55
V_2O_5	0.05	0.24	0.07	0.06	0.06	0.14
SiO_2	0.03	0.08	0.04	0.06	0.12	0.10
TiO_2	0.00	0.00	0.01	0.01	0.00	0.00
Al_2O_3	0.00	0.00	0.00	0.00	0.00	0.00
FeO	0.00	0.02	0.00	0.00	0.00	0.03
MnO	0.00	0.06	0.05	0.09	0.07	0.13
CaO	54.60	55.09	55.33	55.31	53.79	53.94
SrO	1.55	0.32	0.36	0.55	0.47	0.46
F	2.85	2.14	2.28	2.24	2.05	2.21
Cl	0.00	0.00	0.00	0.00	0.00	0.00
H_2O calculated	0.44	0.75	0.65	0.69	0.74	0.67
–O=F	1.20	0.90	0.96	0.94	0.86	0.93
–O=Cl	0.00	0.00	0.00	0.00	0.00	0.00
Total	100.93	100.49	100.40	101.63	99.62	100.52
Structural formulae based on (P + As + V + Si + Ti + Al) = 6 atoms, (Fe + Mn + Ca + Sr) = 10 atoms and (F + Cl + OH) = 2 atoms						
P *apfu*	5.910	5.577	5.402	5.300	5.174	5.089
As	0.080	0.382	0.582	0.682	0.798	0.877
V	0.006	0.027	0.008	0.007	0.007	0.016
Si	0.005	0.014	0.007	0.010	0.021	0.018
Ti	0.000	0.000	0.001	0.001	0.000	0.000
Al	0.000	0.000	0.000	0.000	0.000	0.000
Fe	0.000	0.003	0.000	0.000	0.000	0.004
Mn	0.000	0.009	0.007	0.013	0.010	0.019
Ca	9.849	9.957	9.958	9.934	9.943	9.931
Sr	0.151	0.031	0.035	0.053	0.047	0.046
F	1.512	1.153	1.246	1.213	1.136	1.217
Cl	0.000	0.000	0.000	0.000	0.000	0.000
OH	0.488	0.847	0.754	0.787	0.864	0.783

1: yellow CL zone; 2–6: grey to greenish luminescent zone. * Electron-microprobe data. *apfu*: atoms per formula unit.

Fluorapatite of type II, with a moderate CL emission

Crystals of type-II fluorapatite are anhedral, from 1 to 3 mm in size, appear porous under the microscope, and contain abundant cracks. These crystals occur in late-stage centimetric veinlets, are devoid of inclusions, and contain relict features of growth zoning. They are associated with cryptomelane, Fe-rich braunite, strontian piemontite, aegirine–augite (Morimoto 1989), and rare titanite. In the wider veinlets, fluorapatite occur associated with quartz, albite, manganoan tremolite (Leake *et al*. 1997), hematite, strontian piemontite, Sb-rich rutile and Fe-rich braunite, with numerous inclusions of richterite. The type-II apatite is characterized by numerous cracks, extensive porosity and weaker yellow to green CL emission (Fig. 8), and weak patchy zoning attributed to dissolution and recrystallization. Some crystals present relics of growth zoning (Fig. 9). The CL intensity also is weaker, in some cases completely quenched, and only the Mn^{2+} band at 577 nm is observed (Fig. 10). This type of fluorapatite has the highest Sr content. Sr enrichment in the apatite is linked to the late Sr enrichment of the piemontite and oxides (Perseil 1988, Perseil & Smith 1995). A coupled substitution occurs: As replaces P, and Sr replaces Ca. The As content never exceeds 4%, and V increases with Sr and As (Table 4).

Fluorapatite of type III, with a low CL intensity or none at all

The third type of fluorapatite occurs in late brecciated millimetric veinlets. These crystals also are broken and porous when viewed under the microscope. In some veinlets, brecciated fragments are associated with Sb- and As-rich titanite (Perseil & Smith 1995), skeletal strontian piemontite, roméite, Mn-rich phlogopite and hematite. The CL emission is too weak to photograph with the Technosyn Mark II device. Crystals of type-III fluorapatite are broken and have a high density of

TABLE 3. COMPOSITION* OF TYPE-I FLUORAPATITE FROM THE MICROFISSURES AND LATE-STAGE VEINLETS OF THE ST. MARCEL – PRABORNA DEPOSIT

Sample number	S.M. 96–7 1	2	3	4	5	6
P_2O_5 wt%	42.59	42.74	42.72	42.02	36.54	36.94
As_2O_5	0.17	0.19	0.20	1.01	6.33	6.43
V_2O_5	0.01	0.04	0.00	0.04	0.06	0.02
SiO_2	0.03	0.02	0.01	0.01	0.66	0.34
TiO_2	0.00	0.02	0.03	0.00	0.00	0.00
Al_2O_3	0.00	0.00	0.00	0.00	0.02	0.00
FeO	0.02	0.02	0.04	0.00	0.01	0.01
MnO	0.22	0.47	0.50	0.37	0.06	0.03
CaO	55.17	55.22	55.08	55.35	52.92	52.34
SrO	0.32	0.22	0.17	0.16	0.87	0.84
F	2.55	2.51	2.69	2.52	1.87	1.86
Cl	0.00	0.00	0.00	0.00	0.00	0.00
H_2O calculated	0.59	0.62	0.53	0.60	0.84	0.84
–O=F	1.07	1.06	1.13	1.06	0.79	0.78
–O=Cl	0.00	0.00	0.00	0.00	0.00	0.00
Total	100.60	101.01	100.83	101.02	99.40	98.87
Structural formulae based on (P + As + V + Si + Ti + Al) = 6 atoms, (Fe + Mn + Ca + Sr) = 10 atoms and (F + Cl + OH) = 2 atoms						
P *apfu*	5.979	5.973	5.977	5.906	5.311	5.363
As	0.015	0.016	0.017	0.088	0.568	0.577
V	0.001	0.004	0.000	0.004	0.007	0.002
Si	0.005	0.003	0.002	0.002	0.113	0.058
Ti	0.000	0.002	0.004	0.000	0.000	0.000
Al	0.000	0.000	0.000	0.000	0.001	0.000
Fe	0.003	0.003	0.006	0.000	0.001	0.001
Mn	0.031	0.067	0.071	0.052	0.009	0.004
Ca	9.935	9.909	9.907	9.932	9.902	9.908
Sr	0.031	0.021	0.017	0.016	0.088	0.086
F	1.345	1.318	1.415	1.328	1.024	1.022
Cl	0.000	0.000	0.000	0.000	0.000	0.000
OH	0.655	0.682	0.585	0.672	0.976	0.978

1–4: brightly luminescent zones, 5 and 6: light grey very weakly luminescent zones close to microcracks. * Electron-microprobe data. *apfu*: atoms per formula unit.

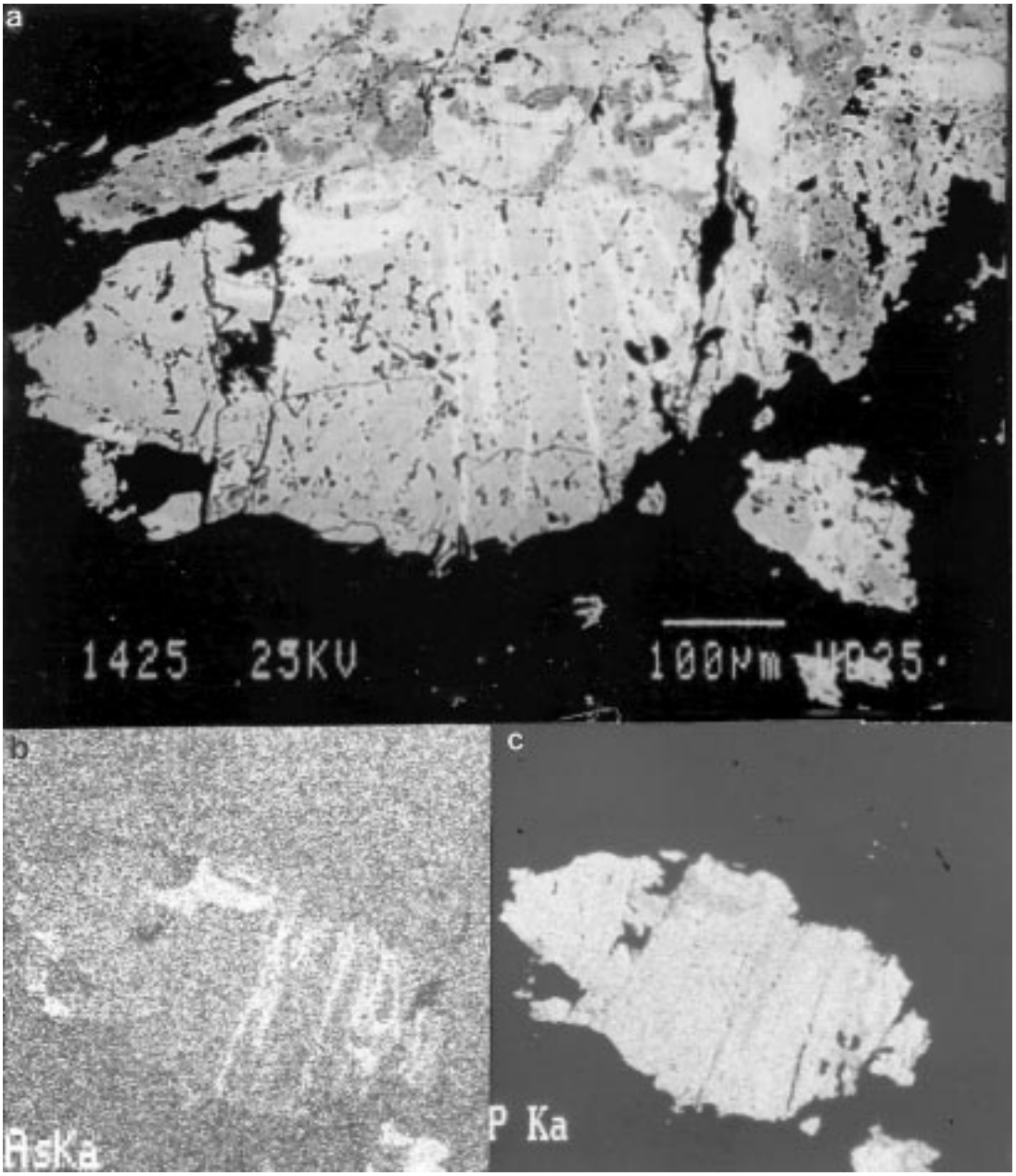

FIG. 6. Images of fluorapatite of type I corresponding to the yellow CL fluorapatite on Figure 1f. Note the contrast between the primary apatite and the compositionally modified apatite along the fractures, and the patchy zoning due to replacement and recrystallization shown on the BSE image (a). b. As X-ray map. c. P X-ray map.

cracks. In some cases, growth zoning is preserved in these grains. As in the type-II apatite, the CL emission is light yellow to green or grey (Figs. 11a, b). The CL intensity is weak, and only the Mn^{2+} band is observed at 577 nm. BSE images reveal that the As content increases close to the rim, the microcracks, and in the dislocations (Figs. 12, 13). Analyses show also that the edges of the cracks are enriched in As (Table 5). These highly

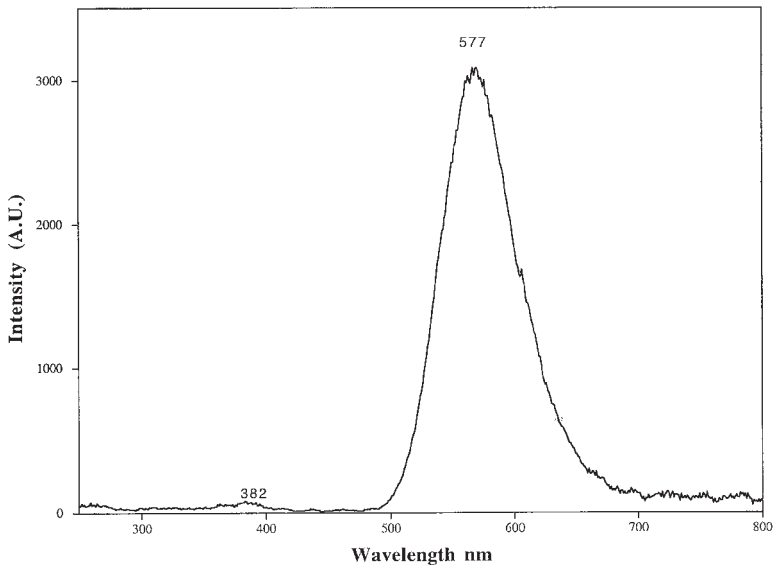

FIG. 7. CL spectrum of the bright yellow CL emission of the primary fluorapatite of Figure 6. Same operating conditions as Figure 4.

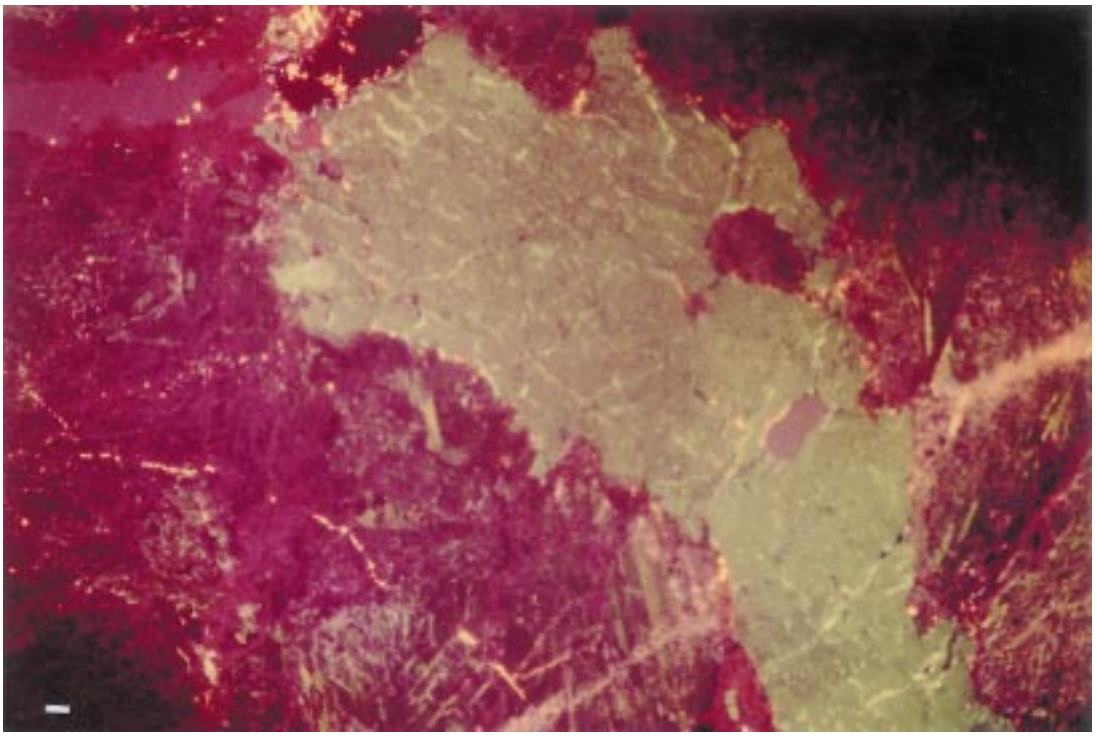

FIG. 8. CL microphotograph of fluorapatite of type II (sample S.M. 7090) with a pale yellow-green hue. The scale bar in the lower left corner is 100 μm.

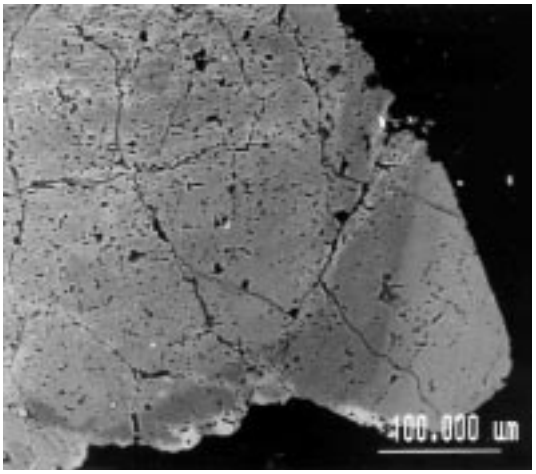

FIG. 9. BSE image of fluorapatite of type II (sample S.M. 7090) showing a porous aspect and relics of the oscillatory growth-zones.

TABLE 4. COMPOSITION* OF TYPE-II FLUORAPATITE FROM A FAULTED LATE-STAGE VEINLET IN THE ST. MARCEL – PRABORNA DEPOSIT

Sample number	S.M. 7090 1	2	3	4	5	6
P_2O_5 wt%	41.70	41.54	39.23	38.05	38.15	37.73
As_2O_5	0.91	1.46	2.54	3.41	3.58	3.43
V_2O_5	0.05	0.03	0.03	0.10	0.19	0.16
SiO_2	0.03	0.06	0.12	0.33	0.08	0.21
TiO_2	0.00	0.01	0.06	0.04	0.03	0.00
Al_2O_3	0.00	0.00	0.00	0.03	0.00	0.02
FeO	0.00	0.00	0.00	0.06	0.07	0.02
MnO	0.00	0.07	0.01	0.19	0.00	0.02
CaO	54.60	53.81	53.40	52.11	51.12	51.08
SrO	1.55	1.72	2.83	4.42	4.88	5.35
F	2.85	2.65	1.90	2.10	2.03	2.03
Cl	0.00	0.00	0.00	0.00	0.00	0.00
H_2O calculated	0.44	0.53	0.85	0.74	0.76	0.75
–O=F	1.20	1.12	0.80	0.88	0.85	0.85
–O=Cl	0.00	0.00	0.00	0.00	0.00	0.00
Total	100.93	100.76	100.16	100.69	100.03	99.95
Structural formulae based on (P + As + V + Si + Ti + Al) = 6 atoms, (Fe + Mn + Ca + Sr) = 10 atoms and (F + Cl + OH) = 2 atoms						
P *apfu*	5.910	5.858	5.739	5.614	5.634	5.628
As	0.080	0.127	0.229	0.311	0.326	0.316
V	0.006	0.003	0.003	0.012	0.022	0.019
Si	0.005	0.010	0.021	0.058	0.014	0.037
Ti	0.000	0.001	0.008	0.005	0.004	0.000
Al	0.000	0.000	0.000	0.001	0.000	0.001
Fe	0.000	0.000	0.000	0.009	0.010	0.003
Mn	0.000	0.010	0.001	0.027	0.000	0.003
Ca	9.849	9.820	9.720	9.527	9.499	9.458
Sr	0.151	0.170	0.279	0.437	0.491	0.536
F	1.512	1.409	1.032	1.149	1.118	1.123
Cl	0.000	0.000	0.000	0.000	0.000	0.000
OH	0.488	0.591	0.968	0.851	0.882	0.877

1: weakly luminescent zone, 2–6: very weakly luminescent zones. * Electron-microprobe data. *apfu*: atoms per formula unit.

TABLE 5. COMPOSITION* OF TYPE-III FLUORAPATITE FROM A MICROFISSURED AND FAULTED LATE-STAGE VEINLET, ST. MARCEL – PRABORNA DEPOSIT

Sample number	S.M. 93 1	2	3	4	5	6
P_2O_5 wt%	41.18	39.62	39.11	37.02	35.88	35.27
As_2O_5	1.17	2.70	2.91	6.24	7.21	7.72
V_2O_5	0.00	0.07	0.01	0.06	0.04	0.00
SiO_2	0.06	0.08	0.09	0.02	0.02	0.16
TiO_2	0.00	0.01	0.02	0.00	0.00	0.02
Al_2O_3	0.00	0.00	0.00	0.01	0.02	0.01
FeO	0.00	0.10	0.00	0.00	0.00	0.01
MnO	0.03	0.06	0.03	0.05	0.06	0.00
CaO	54.67	53.90	53.00	54.02	53.96	53.80
SrO	0.92	0.67	2.89	1.11	1.17	1.16
F	2.34	2.14	2.23	2.16	2.13	2.22
Cl	0.00	0.00	0.00	0.00	0.00	0.00
H_2O calculated	0.66	0.74	0.69	0.72	0.72	0.67
–O=F	0.99	0.90	0.94	0.91	0.90	0.93
–O=Cl	0.00	0.00	0.00	0.00	0.00	0.00
Total	100.05	99.18	100.04	100.50	100.31	100.10
Structural formulae based on (P + As + V + Si + Ti + Al) = 6 atoms, (Fe + Mn + Ca + Sr) = 10 atoms and (F + Cl + OH) = 2 atoms						
P *apfu*	5.887	5.736	5.718	5.425	5.330	5.258
As	0.103	0.241	0.263	0.565	0.661	0.711
V	0.000	0.008	0.001	0.007	0.005	0.000
Si	0.010	0.014	0.016	0.003	0.004	0.028
Ti	0.000	0.001	0.003	0.000	0.000	0.003
Al	0.000	0.000	0.000	0.000	0.001	0.000
Fe	0.000	0.014	0.000	0.000	0.000	0.001
Mn	0.004	0.009	0.004	0.007	0.009	0.000
Ca	9.905	9.910	9.709	9.883	9.875	9.883
Sr	0.090	0.067	0.287	0.110	0.116	0.115
F	1.251	1.159	1.214	1.176	1.169	1.224
Cl	0.000	0.000	0.000	0.000	0.000	0.000
OH	0.749	0.841	0.786	0.824	0.831	0.776

1–3: very weakly luminescent zones, 4–6: dull zones. * Electron-microprobe data. *apfu*: atoms per formula unit.

disrupted crystals of fluorapatite are generally associated with As- and Sb-bearing titanite (Perseil & Smith 1995). Contrary to fluorapatite of type II, the Sr content does not seem to be linked to the substitution of P by As.

INFLUENCE OF CRYSTAL CHEMISTRY OF As-BEARING FLUORAPATITE ON INTENSITY OF CATHODOLUMINESCENCE

In the fluorapatite from St. Marcel – Praborna, As contents are as high as 9.55 wt% As_2O_5. Similar high values (up to 13.8 wt%) were reported recently in apatite from Mn ores from quartz-rich pink schists from the Starlera deposit, Val Ferrera (Brugger & Gieré 1999). The main substitution in the tetrahedral position is that of P by As. Arsenic can occupy one-sixth of the P content in apatite (Fig. 14a). The least-luminescent examples of fluorapatite are the richest in As; the very bright yellow luminescent fluorapatite of type I has prac-

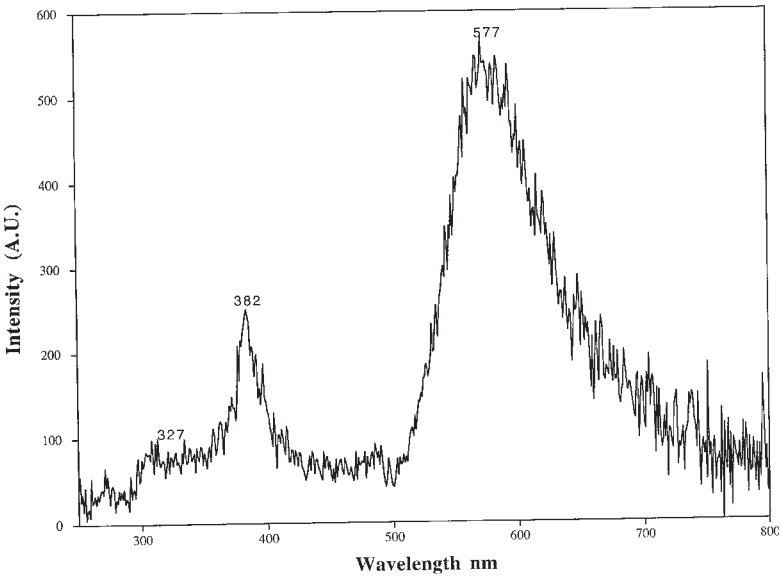

FIG. 10. CL spectrum of the most intense zone of the fluorapatite of Figure 9. Same operating conditions as in Figure 4.

tically no As in the tetrahedral site. Sr content is as high as 5.35 wt% SrO, and similar values are reported in apatite from lamproite (Edgar 1989). Sr is the main cation replacing Ca in the polyhedra (Fig. 14b). The highest Sr contents are found in the least-luminescent grains of apatite, but apatite exhibiting very intense cathodoluminescence or no luminescence may have similar Sr and Ca contents (Fig. 14b). Besides Sr, which occupies only the Ca(1) site, Mn is the second most abundant cation, and it may occupy both Ca sites (Hughes *et al.* 1991a). The sum Mn + Sr displays an excellent correlation with Ca content (Fig. 14c), indicating that the other cations such as the *REE* are only accessory in these sites. No correlations exist between Mn and Ca (Fig. 14c). Very strongly luminescent fluorapatite is the richest in Mn (Fig. 14d), but luminescent and nonluminescent apatite plot together at low Mn values (Fig. 14d). The weakly luminescent and non-luminescent apatite are

TABLE 6. CONCENTRATIONS OF TRACE ELEMENTS IN FLUORAPATITE FROM THE ST. MARCEL – PRABORNA DEPOSIT

Sample	S.M. 23–1					S.M. 98–2		S.M. 96–7				S.M. 7090					S.M. 93				
number	1	2	3	4	5	6	7	8	9	10	11	12	13	14	15	16	17	18	19	20	21
V ppm	25	118	217	46	36	289	169	54	154	96	86	129	515	67	169	239	10	58	81	86	30
Mn	69	89	37	44	68	362	761	2348	1863	2053	2062	770	676	661	668	567	520	235	253	249	313
Y	58	27	40	70	110	106	95	47	75	34	121	232	446	139	365	544	84	53	32	30	30
Ce	182	198	92	89	57	68	57	17	65	28	95	210	78	97	140	148	92	71	32	27	29
Nd	76	49	225	85	163	40	35	20	52	69	263	122	258	113	163	344	131	243	243	50	248
Sm	193	193	20	165	193	868	770	695	570	688	636	120	238	75	95	106	571	719	892	847	793
Eu	74	207	133	202	111	118	176	11	57	88	8	196	176	97	245	70	134	68	32	176	181
Gd	107	16	108	243	270	92	184	165	41	13	46	101	66	192	139	311	120	149	97	93	92
Tb	123	137	83	58	69	71	42	50	52	17	28	24	78	3	19	38	3	104	57	60	80
Dy	115	206	100	176	60	96	106	106	17	36	98	80	208	169	122	128	102	65	82	118	98
Tm	1	206	92	211	115	7	170	186	82	58	104	106	212	196	174	44	105	54	171	174	61
Yb	90	120	10	124	108	25	13	114	8	61	31	60	78	111	59	113	28	71	106	24	15

Columns 1 to 5 pertain to compositions 1 to 5 from Table 1. Columns 6 and 7 pertain to compositions 1 and 2 from Table 2. Columns 8 to 11 pertain to compositions 1, 2, 3 and 4 from Table 3. Columns 12 to 16 pertain to compositions 1 to 5 from Table 4. Columns 17 to 21 pertain to compositions 1 to 5 from Table 5.

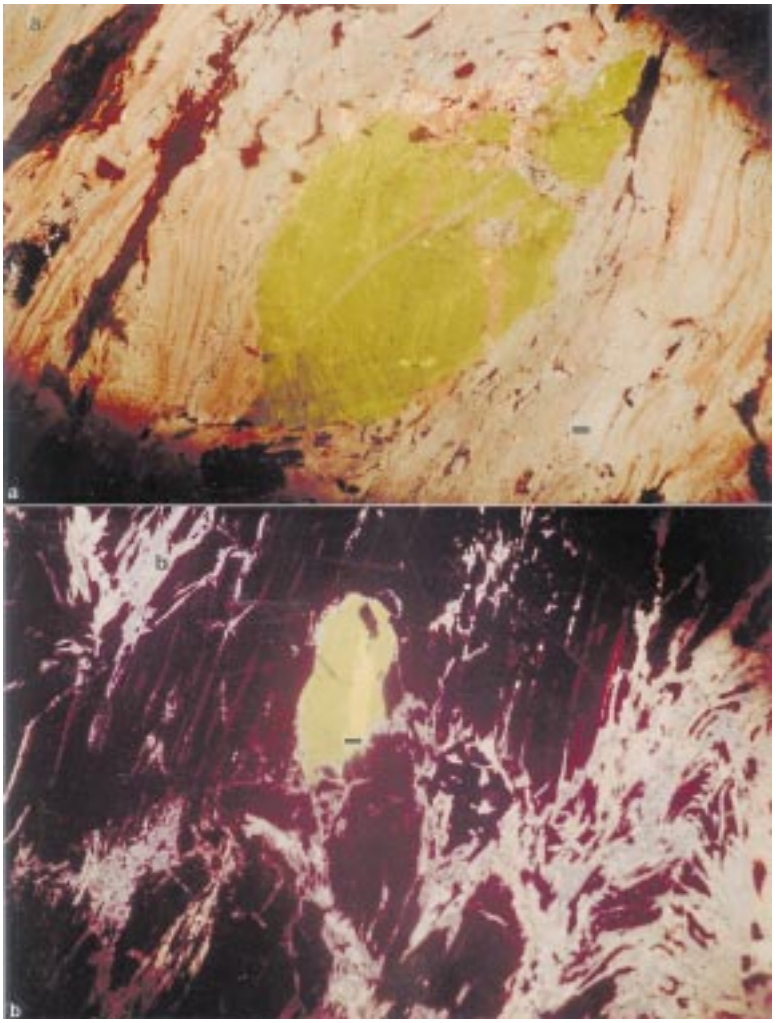

FIG. 11. CL microphotograph of fluorapatite of type III (sample S.M. 93) with a pale green hue (a) associated with pale orange carbonate and feldspar. In the second apatite of type III (b), the green dislocated mineral presents a yellow oscillatory growth-zone, which is a relic of the primary apatite. The pink to pale orange luminescent feathery minerals are calcite and albite.Width of photographs : 5.1 mm.

also the least fluorine-rich (Fig. 14e), and more enriched in As and OH (Fig. 14f). The same correlation between F and As was observed by Brugger & Gieré (1999).

If Mn-rich fluorapatite is invariably luminescent, Mn-poor apatite can have a bright luminescence only if it contains less than 0.12 atoms per formula unit (*apfu*) of As, and the very weakly luminescent to nonluminescent crystals of apatite contain less than 0.55 *apfu* As (Figs. 14a, 15a). In sector-zoned topaz from San Luis Potosi, Mexico, Northrup & Reeder (1994) observed different As concentrations within the various subsectors. The incorporation of up to 40 ppm As seems to play a role on the yellow CL emission of the subsector of the topaz. In the case of the fluorapatite, such low concentrations of As could also play a similar role in CL *via* an energy-transfer process; however, the drastic increase in As quenches all luminescence, probably as a result of defect-related phenomena. On the contrary, luminescence intensity is not coupled with the *REE* content (Fig. 15b).

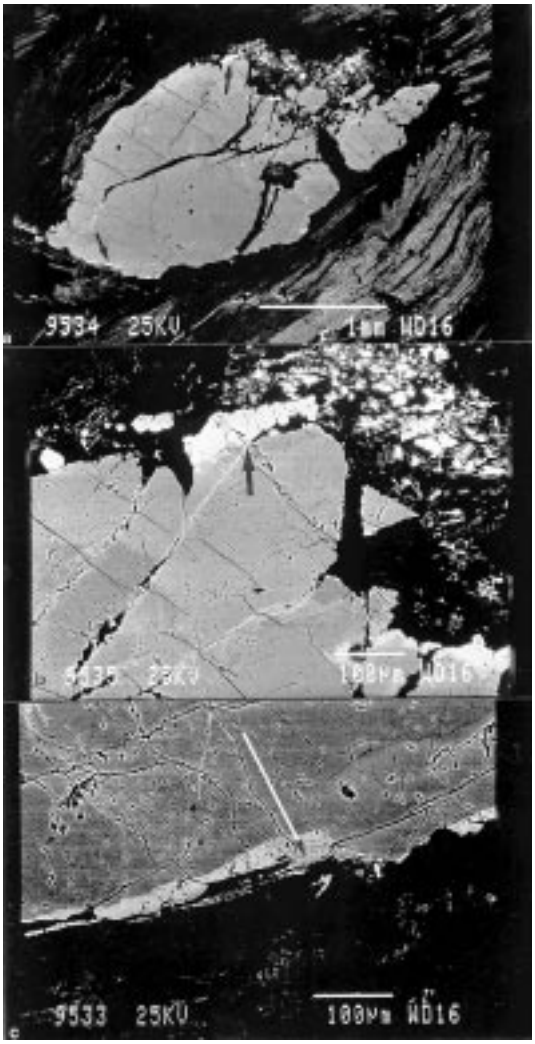

FIG. 12. BSE images of fluorapatite of type III (sample S.M. 93) corresponding to the pale green CL emission of the fluorapatite in Figure 11a. The detailed BSE images (b and c) correspond to the enlargement of the areas in 12a shown by arrows. In b, the bright outer zone is the most enriched in As. As occur also along the microcracks (light grey). The bright white skeletal crystals are titanite. The same features are observed in the lower part of the fluorapatite crystal (c).

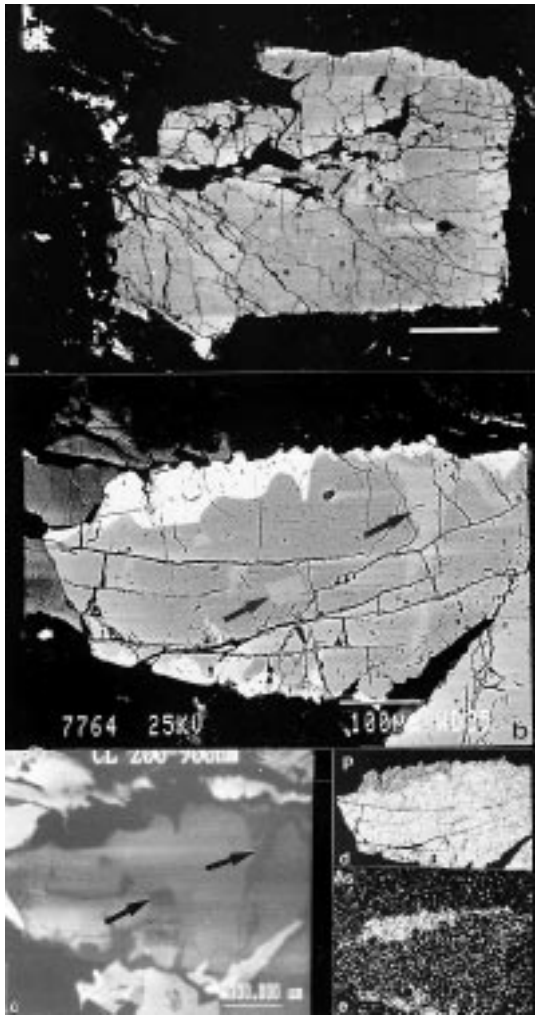

FIG. 13. Highly fractured fluorapatite of type III (sample S.M.93). Note that the bright white zones enriched in As are close to the border of the crystal and along the microcracks in light grey (BSE image, a). A detail of the upper border of the crystal (small arrow) is given in b, showing the irregular enrichment of the rim in As (white), as well as the trace of As circulating fluids along the cracks (light grey). On the contrary, the As-rich zones are dull in the CL image (c), and the microcracks, shown by the arrows, are less luminescent than the primary apatite. The replacement of P (d) by As (e) is illustrated in the X-ray maps.

The role of As in the quenching phenomenon is obvious, but the mechanism is still debated. It is probable, as proposed by Hughes & Drexler (1991), that disorder in fermorite can be induced by As substituting for P in the tetrahedral site, owing to the very different size, 0.335 Å for ^{IV}As and 0.17 Å for ^{IV}P (Shannon 1976), although this happens without causing major structural distortions in the apatite structure (Hughes & Drexler 1991). However, this small disruption in the atomic arrangement is perhaps sufficient to quench the luminescence phenomenon. The disorder due to [AsO_4] vibration was also observed by Raman spectroscopy (Perseil & Smith 1999). Disorder due to As can also

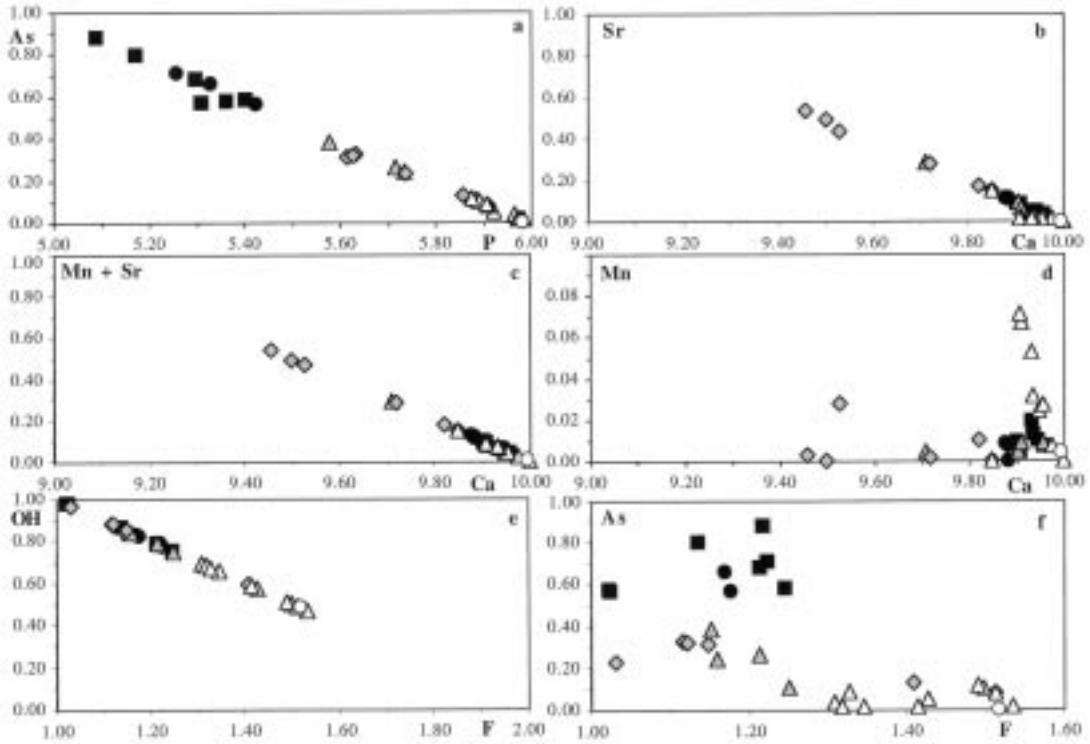

FIG. 14. Element correlations in fluorapatite from St. Marcel – Praborna. Open circle: very bright yellow luminescent fluorapatite, open triangle: brightly luminescent fluorapatite, grey diamond: less intensely luminescent apatite, grey triangle: weakly luminescent fluorapatite, square: very weakly luminescent areas, dots: dull zones. a: As *versus* P; b: Sr *versus* Ca; c: Mn + Sr *versus* Ca; d: Mn *versus* Ca; e: OH *versus* F; f: As *versus* F.

change the position of the anion (Fig. 14f), the OH species being disordered compared to F (Hughes *et al.* 1989).

CONCLUSIONS

The quenching effect of the Mn^{2+} peak by Fe^{2+} has been demonstrated on synthetic carbonate fluorapatite (Filippelli & Delaney 1993). The As-bearing fluorapatite of St. Marcel – Praborna shows a high *REE* content and iron commonly below the detection limit of the electron microprobe. However, the presence of As in the apatite structure quenches first the sharp *REE* emission lines corresponding to the *f–f* electronic transitions. It affects less the broad Mn^{2+} emission band corresponding to the *d–d* electronic transition. However, with the strong increase of the As content, up to 10 wt% As_2O_5, the emission due to Mn^{2+} is also completely quenched. The increase of the As content in the fluorapatite of type II and III from St. Marcel – Praborna, with inferred slight distortions in the structure of the apatite, could be responsible for the quenching of the luminescence observed in these samples. The presence of As-bearing fluorapatite at this locality is related to fracturing of the minerals and linked to late circulation of fluid enriched in As and Sr.

ACKNOWLEDGEMENTS

We thank M. Fialin and H. Rémy (Centre de Microanalyses Camparis, Université Pierre et Marie Curie, Paris VI) for help with the electron microprobe. This research was supported by grants from the Fédération de Recherche (FR 32–CNRS) through the project "Apatite", under the supervision of Dr. C. Wagner. Mrs. M. Marot from the Muséum National d'Histoire Naturelle is thanked for the preparation of thin sections. The electron-microprobe analyses and the SEM and CL studies were funded by FR 32, and by funds of the different laboratories at the Muséum National d'Histoire Naturelle, the Université de Paris VI and the CRPG–CNRS Nancy. We thank Drs. W.L. Brown and L. Shengold (both at CRPG–CNRS Nancy) for correcting the English. Drs. J. Murray of Stanford University, J.M. Hughes, of Miami University, and an anonymous reviewer provided constructive reviews. The manuscript

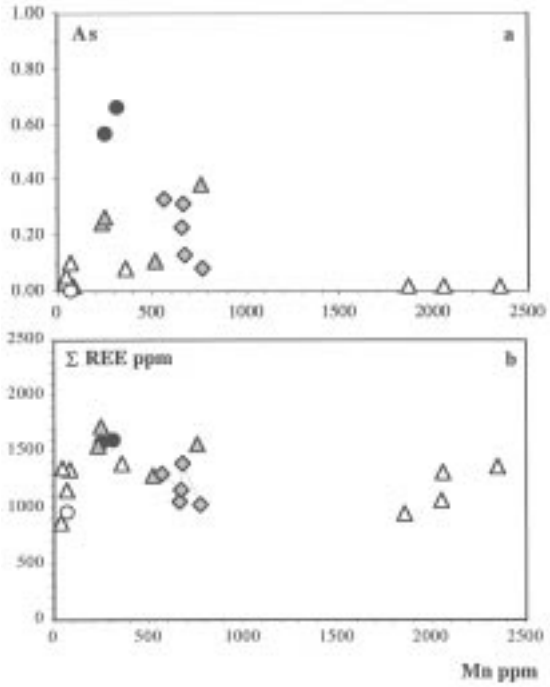

FIG. 15. Element correlations in fluorapatite from St. Marcel – Praborna. a. As (*apfu*) *versus* Mn expressed in ppm. b. Sum of the *REE versus* Mn, both expressed in ppm.

was also greatly improved by the comments and suggestions of the editor.

REFERENCES

BLANC, P., BAUMER, A., CESBRON, F. & OHNENSTETTER, D. (1995): Les activateurs de cathodoluminescence dans des chlorapatites préparées par synthèse hydrothermale. *C.R. Acad. Sci. Paris, sér.* **II**, **321**, 1119-1126.

BROWN, P., ESSENE, E.J. & PEACOR, D.R.. (1978): The mineralogy and petrology of manganese-rich rocks from St. Marcel, Piedmont, Italy. *Contrib. Mineral. Petrol.* **67**, 227-232.

BRUGGER, J. & GIERÉ, R. (1999): As, Sb, Be and Ce enrichment in minerals from a metamorphosed Fe–Mn deposit, Val Ferrera, eastern Swiss Alps. *Can. Mineral.* **37**, 37-52.

BURCKHARDT, C.E. & FALINI, F. (1956): Memoria sui giacimenti italiani di manganese. *Int. Geol. Congress 20th* (*Mexico*) *Symposium sobre yacimientos de manganeso* (J. González Reyna, ed.) **V**, 221-272.

DAL PIAZ, G.V., DI BATTISTINI, G., KIENAST, J.R. & VENTURELLI, D.R. (1979): Manganiferous quartzitic schists of the Piemonte ophiolite nappe in the Valsesia–Valtournanche area (Italian Western Alps). *Mém. Sci. Géol.* **32**.

DEBENEDETTI, A. (1965): Il complesso radiolariti – giacimenti di manganese – giacimenti piritoso – cupriferi – rocce a fuchsite, come rappresentate del Malm nella Formazione dei Calcescisti. Osservazioni nelle Alpi Piemontesi e nella Valle d'Aosta. *Bol. Soc. Geol. Ital.* **84**, 3-35.

DRAKE, M.J. & WEILL, D.F. (1972): New rare earth element standards for electron microprobe analysis. *Chem. Geol.* **10**, 179-191.

DUNN, P.J., PEACOR, D.R. & NEWBERRY, N. (1980): Johnbaumite, a new member of the apatite group from Franklin, New Jersey. *Am. Mineral.* **65**, 1143-1145.

EDGAR, A.D. (1989): Barium-and strontium-enriched apatites in lamproites from West Kimberley, Western Australia. *Am. Mineral.* **74**, 889-895.

EFIMOV, A.F., KRAVCHENKO, S.M. & VASIL'EVA, Z.V. (1962): Strontium apatite – a new mineral. *Dokl. Akad. Nauk SSSR* **142**, 439-442 (in Russ.).

ELLIS, D.J. & GREEN, D.H. (1979): An experimental study of the effect of Ca upon garnet – clinopyroxene Fe–Mg exchange equilibria. *Contrib. Mineral. Petrol.* **71**, 13-22.

ERNST, W. G. & DAL PIAZ, G.V. (1978): Mineral parageneses eclogitic rocks and related mafic schists of the Piemonte ophiolite nappe, Breuil – St-Jacques area, Italian Western Alps. *Am. Mineral.* **63**, 621-640.

FIALIN, M., OUTREQUIN, M. & STAUB, P.F. (1997): A new tool to peak overlaps in electron-probe microanalysis of rare-earth-element L-series X-rays . *Eur. J. Mineral.* **9**, 965-968.

FILIPPELLI, G.M. & DELANEY, M.L. (1993): The effect of manganese (II) and iron (II) on the cathodoluminescence signal in synthetic apatite. *J. Sed. Petrol.* **63**, 167-173.

FLEET, M.E. & PAN, YUANMING (1995): Site preference of rare earth elements in fluorapatites. *Am. Mineral.* **80**, 329-335.

GAFT, M., REISFELD, R., PANCZER, G., SHOVAL, S., CHAMPAGNON, B. & BOULON, G. (1997): Eu^{3+} luminescence in high-symmetry sites of natural apatite. *J. Lumin.* **72-74**, 572-574.

HOLLAND, T.J.B. (1980): The reaction albite = jadeite + quartz determined experimentally in the range 600–1200°C. *Am. Mineral.* **65**, 129-134.

HUEBNER, J. (1977): The manganese oxides – a bibliographic commentary. *In* Oxide minerals (D. Rumble, ed.). *Mineral. Soc. Am., Short Course Notes*, SH1-SH17.

HUGHES, J.M., CAMERON, M. & CROWLEY, K.D. (1989): Structural variations in natural F, OH, and Cl apatites. *Am. Mineral.* **74**, 870-876.

_____, _____ & _____ (1991a): Ordering of divalent cations in the apatite structure: crystal structure refinements of natural Mn- and Sr-bearing apatite. *Am. Mineral.* **76**, 1857-1862.

_____ , _____ & MARIANO, A.N. (1991b): Rare-earth-element ordering and structural variations in natural rare-earth-bearing apatite. *Am. Mineral.* **76**, 1165-1173.

_____ & DREXLER, J.W. (1991): Cation substitution in the apatite tetrahedral site: crystal structures of type hydroxyellestadite and type fermorite. *Neues Jahrb. Mineral., Monatsh.*, 327-336.

LEAKE, B.E. and 21 others (1997): Nomenclature of amphiboles: report of the Subcommittee on Amphiboles of the International Mineralogical Association, Commission on New Minerals and Mineral Names. *Can. Mineral.* **35**, 219-246.

MARFUNIN, A.S. (1979): *Spectroscopy, Luminescence and Radiation Centres in Minerals.* Springer- Verlag, Berlin, Germany.

MARIANO, A.N. & RING, P.J. (1975): Europium activated cathodoluminescence in minerals. *Geochim. Cosmochim. Acta* **39**, 649-660.

MARSHALL, D.J. (1988): *Cathodoluminescence of Geological Materials*. Unwin Hyman, Boston, Massachusetts.

MARTIN-VERNIZZI, S. (1982): *La mine de Praborna* (*Val d'Aoste, Italie*): *une série manganésifère métamorphisée dans le facies éclogite*. Thèse 3ème cycle, Université Pierre et Marie Curie, Paris VI, France.

MARTIN, S. & KIENAST, J.R. (1987): The HP–LT manganiferous quartzites of Praborna, Piemonte ophiolite nappe, Italian Western Alps. *Schweiz. Mineral. Petrogr. Mitt.* **67**, 339-360.

MITCHELL, R.H., XIONG, JIAN, MARIANO, A.N. & FLEET, M.E. (1997): Rare-earth-element-activated cathodoluminescence in apatite. *Can. Mineral.* **35**, 979-998.

MORIMOTO, N. (1989): Nomenclature of pyroxenes. *Can. Mineral.* **27**, 143-156.

MOROZOV, A.M., MOROZOVA, L.G., TREFIMOV, A.K. & FEOFILOV, P.P. (1970): Spectral and luminescent characteristics of fluoroapatite single crystals activated by rare earth ions. *Optika i Spektroskopia* **29**, 590-596.

MOTTANA, A. (1986): Blueschist-facies metamorphism of manganiferous cherts: a review of the alpine occurrences. *Geol. Soc. Am., Mem.* **164**, 267-299.

NORTHRUP, P.A. & REEDER, R.J. (1994): Evidence for the importance of growth-surface structure to trace element incorporation in topaz. *Am. Mineral.* **79**, 1167-1175.

PERSEIL, E.A. (1988): La présence de strontium dans les oxydes manganésifères du gisement de St. Marcel – Praborna (Val d'Aoste, Italie). *Mineral. Deposita* **23**, 271-276.

_____ (1991): La présence de Sb-rutile dans les concentrations manganésifères de St. Marcel – Praborna (V. Aoste, Italie). *Schweiz. Mineral. Petrogr. Mitt.* **71**, 306-308.

_____ & SMITH, D.C. (1995): Sb-rich titanite in the manganese concentrations at St. Marcel – Praborna, Aosta Valley, Italy: petrography and crystal chemistry. *Mineral. Mag.* **59**, 717-734.

_____ & _____ (1996): Cristallochimie de l'arsenic dans la fluorapatite et la titanite des concentrations manganésifères de St. Marcel – Praborna (Italie). *16ème Réunion Sci. de la Terre* (*Orléans*), 167 (abstr.).

_____ & _____ (1999): Raman spectra of arsenic-bearing fluorapatite from St. Marcel (Italy) and of type fermorite: $(Ca,Sr)_5([AsO_4],[PO_4])_3(OH,F)$. *Georaman'99, 14th International Conference* (*Valladolid*), *abstr.*

PETERS, T.J., TROMMSDORFF, V. & SOMMERAUER, J. (1978): Manganese pyroxenoids and carbonates. Critical phase relations in metamorphic assemblages from the Alps. *Contrib. Mineral. Petrol.* **66**, 383-388

PORTNOV, A.M. & GOROBETS, B.S. (1969): Luminescence of apatite from different rock types. *Dokl. Akad. Nauk SSSR* **184**, 110-115 (in Russ.).

POUCHOU, J.-L. & PICHOIR, F. (1991): Quantitative analysis of homogeneous or stratified microvolumes applying the model "PAP". *In* Electron Probe Quantitation (K.F.J. Heinrich & D.E. Newbury, eds.). Plenum Press, New York, N.Y. (31-75).

REMOND, G., CESBRON, F., CHAPOULIE, R., OHNENSTETTER, D., ROQUES-CARMES, C. & SCHVOERER, M. (1992): Cathodoluminescence applied to microcharacterization of mineral materials: a present status in experimentation and interpretation. *Scanning Microscopy* **6**, 23-68.

ROEDER, P.L., MACARTHUR, D., MA, XIN-PEI, PALMER, G.L. & MARIANO, A.N. (1987): Cathodoluminescence and microprobe study of rare-earth elements in apatite. *Am. Mineral.* **72**, 801- 811.

RØNSBO, J.G. (1989): Coupled substitution involving REEs and Na and Si in apatites in alkaline rocks from the Ilimaussaq intrusion, South Greenland, and the petrological implications. *Am. Mineral.* **74**, 896-901.

SHANNON, R.D. (1976): Revised effective ionic radii and systematic studies of inter-atomic distances in halides and chalcogenides. *Acta Crystallogr.* **A32**, 751-767.

TARASHCHAN, A.N. (1978): *Luminescence of Minerals*. Naukowa Dumka, Kiev, Ukraine (in Russ.).

VELDE, B. (1967): Si^{4+} content of natural phengites. *Contrib. Mineral. Petrol.* **14**, 250-258.

WHITNEY, J.A. & STORMER, J.C. (1977): The distribution of $NaAlSi_3O_8$ between coexisting microcline and plagioclase and its effect on geothermometric calculations. *Am. Mineral.* **62**, 687-691.

Received August 10, 1999, revised manuscript accepted February 17, 2000.

APPENDIX: ANALYTICAL METHODS

Cathodoluminescence imaging was done using a cold-cathode (Marshall 1988, Remond *et al.* 1992) Technosyn Mark II device mounted on a Nikon Optiphot optical microscope at the Université de Paris VI. The working conditions were: accelerating voltage 15 kV, beam current 0.5 mA, photographic film, Kodak Ektachrome P1600x EPH 135–36.

Complementary CL images were obtained on a scanning electron microscope (SEM) and are compared to secondary electron (SE) and back-scattered electron (BSE) images. Cathodoluminescence spectra (Blanc *et al.* 1995) were recorded from 200 to 900 nm with a CL spectrometer attached to a JEOL JSM 840A scanning electron microscope at the Université de Paris VI, using the following equipment: an aluminum-plated parabolic mirror collector, silica lens suitable for ultra-violet (UV) transmission, a Jobin–Yvon H10.UV grating spectrometer, and a Hamamatsu R636 AsGa photomultiplier with a 650 U curve. The operating conditions for CL spectrometry were: voltage: 25 kV, beam intensity: usually 1×10^{-7} A, spectrometer slits: 1 mm, scan step: 1 nm, integration time: 0.2 s. The wavelength domain analyzed is from 200 to 900 nm, which permits spectra from the UV to the infrared (IR) to be recorded; this is a significant improvement compared to other CL devices, which are blind in the UV region. The spectra were corrected for the spectral response function of the spectrometer and detector. Minerals were photographed by BSE and CL on the same SEM.

Electron-microprobe analyses (EPMA) were done using the Cameca SX–50 wavelength-dispersion instrument at Camparis – Université de Paris VI. The analytical conditions were: acceleration voltage: 15 kV, beam current: 15 nA, counting time: 10 s per element on peaks and backgrounds. Concentrations of As, Mn, Fe, V, Sr, Y and the *REE* were established under the following conditions: acceleration voltage 25 kV, beam current 50 nA, with each result the mean of 10 measurements, each counting time being 200 s on peaks and backgrounds. The *REE* peak-overlap treatment uses the Fialin *et al.* (1997) on-line procedure. The following standards were used: fluorapatite for Ca*K*α, P*K*α and F*K*α, synthetic AsGa for As*L*β, synthetic Sr-bearing silicate for Sr*L*α, orthoclase for Al*K*α, diopside for Si*K*α, vanadinite for V*K*α, synthetic Fe_2O_3 for Fe*K*α, synthetic pyrophanite for Mn*K*α and Ti*K*α, synthetic La_3ReO_8 for La*L*α, synthetic Nd_3ReO_8 for Nd*L*β, synthetic Sm_3ReO_8 for Sm*L*β, synthetic Nd_2Cu_3 for Nd*L*β, synthetic *REE*- and Y-bearing glasses (Drake & Weill 1972) for Ce*L*α, Pr*L*β, Eu*L*β, Gd*L*β, Tb*L*α, Dy*L*β, Er*L*β, Tm*L*β, Yb*L*α and Y*L*α. The Cameca data-reduction program is PAP (Pouchou & Pichoir 1991). The general formula of apatite is $A_{10}(MO_4)_6X_2$, with pentavalent and tetravalent cations in the *M* site, divalent and trivalent cations in the *A* site, and F, OH and Cl in the *X* site. The structural formulae of the apatite were calculated on the basis of 25 atoms of oxygen and 1 H_2O and normalized on (P + Si + Ti + Al + V + As) = 6, (Fe + Mn + Ca + Sr) = 10 and (F + Cl + OH) = 2 *apfu*.